

Article

Computational Insights into the Interaction between Neprilysin and α -Bisabolol: Proteolytic Activity against Beta-Amyloid Aggregates in Alzheimer's Disease

Jonathan Elias Rodrigues Martins ¹, José Ednésio da Cruz Freire ^{1,*}, Francisco Sérgio Lopes Vasconcelos-Filho ^{1,2}, Diego da Silva de Almeida ³, Vânia Marilande Ceccatto ¹  and Bruno Lopes de Sousa ³ 

¹ Biochemistry and Gene Expression Laboratory, Superior Institute of Biomedical Sciences, State University of Ceará, Fortaleza 60714-903, Ceará, Brazil; jonathan.erm11@gmail.com (J.E.R.M.); seergiolopes@hotmail.com (F.S.L.V.-F.); vania.ceccatto@uece.br (V.M.C.)

² Dean of Culture, Federal University of Cariri, Juazeiro do Norte, Fortaleza 63048-080, Ceará, Brazil

³ Faculty of Philosophy Dom Aureliano Matos, State University of Ceará, Limoeiro do Norte, Fortaleza 62930-000, Ceará, Brazil; diegoalmeidasilva081@gmail.com (D.d.S.d.A.); brunolopes.sousa@uece.br (B.L.d.S.)

* Correspondence: jedenesio@gmail.com

Abstract: (1) Background: Alzheimer's disease (AD) is an irreversible disorder of the central nervous system associated with beta-amyloid protein ($A\beta$) deposition and accumulation. Current treatments can only act on symptoms and not the etiologic agent. Neprilysin and α -bisabolol have been shown to reduce the aggregation of $A\beta$, suggesting a potential interaction between both molecules, leading to increased proteolytic activity on $A\beta$ aggregates. (2) Methods: Computational simulations were conducted to explore the interaction between murine neprilysin [NEP(m)] and α -bisabolol and their effects on enzymatic activity. NEP(m) structure was predicted using comparative modeling, and the binding pattern to α -bisabolol and its effects on leu-enkephalin binding were explored through docking calculations and molecular dynamics simulations, respectively. (3) Results: The findings suggest that α -bisabolol stabilizes the Val⁴⁸¹-Pro⁴⁸⁸ segment of NEP2(m), which directly interacts with the peptide substrate, enabling an optimized alignment between the catalytic residue Glu⁵²⁵ and leu-enkephalin. (4) Conclusions: This computational evidence strongly supports the notion that α -bisabolol stabilizes peptide substrates at the NEP2(m) catalytic site, leading to the positive modulation of enzymatic activity.

Keywords: amyloidogenic pathway; levomenol; anti-amyloidogenic



Citation: Martins, J.E.R.; da Cruz Freire, J.E.; Vasconcelos-Filho, F.S.L.; da Silva de Almeida, D.; Ceccatto, V.M.; de Sousa, B.L. Computational Insights into the Interaction between Neprilysin and α -Bisabolol: Proteolytic Activity against Beta-Amyloid Aggregates in Alzheimer's Disease. *Processes* **2024**, *12*, 885. <https://doi.org/10.3390/pr12050885>

Received: 18 March 2024

Revised: 25 April 2024

Accepted: 26 April 2024

Published: 27 April 2024



Copyright: © 2024 by the authors. Licensee MDPI, Basel, Switzerland. This article is an open access article distributed under the terms and conditions of the Creative Commons Attribution (CC BY) license (<https://creativecommons.org/licenses/by/4.0/>).

1. Introduction

Alzheimer's disease (AD) is a prevalent and irreversible disorder of the central nervous system, characterized by the loss of cognitive functions, attention, judgment, and memory. According to the latest statistics, more than 55 million people worldwide are suffering from AD or related dementias [1], and this has generated a significant socioeconomic burden. Taking only individuals with AD in Brazil into account, the average annual cost of treating individuals via the public health system was estimated at USD 4020.47 (the Brazilian currency is the real but was converted into the US dollar), an amount considered relatively high for the country [2]. This makes AD and other dementias the leading cause of disability, especially among elderly populations.

AD is intimately associated with the deposition and accumulation of β -amyloid peptide ($A\beta$) [3]. $A\beta$ is a highly toxic peptide for neurons [4], and its buildup can result in the formation of oligomers and amyloid plaques. Two isoforms of $A\beta$, $A\beta_{1-42}$, and $A\beta_{1-40}$ peptides are the primary components of these amyloid plaques [5]. From the clinical-biological point of view, abnormalities linked to cerebral amyloid peptides are observed in the early

stages of AD, where the levels of the $A\beta_{1-42}$ peptide decrease (showing an $A\beta_{1-42}/A\beta_{1-40}$ ratio) in the cerebrospinal fluid. Interestingly, the pathway of plaque formation remains unknown. However, some clues seem to be associated with the predominant presence of both $A\beta$ isoforms in these plaques despite $A\beta_{1-40}$ comprising approximately 90% of the $A\beta$ pool [6]. Evidence suggests that a more significant hydrophobic potential is induced due to additional amino acids in the $A\beta_{1-42}$ isoform, resulting in a sufficiently strong hydrophobicity for the chains to undergo liquid–liquid phase separation into condensates of fibers. This effect provides theoretical support for the hypothesis that LLPS condensates act as precursors for aggregation and forming $A\beta$ plaques through hydrophobic interactions. This makes it possible to define the stage known as the “Alzheimer’s continuum” [7] before the occurrence of the anomalies (hyperphosphorylation) found in the Tau protein (p-Tau). This, in turn, leads to the detachment of Tau from microtubules, resulting in the destabilization of axonal microtubule scaffolds, impairments in axonal transport [8], and eventually neuronal death.

The $A\beta$ pathway presents the enzyme neprilysin, NEP2(m), a membrane metallopeptidase belonging to the M13 family. The NEPs are also known by different nomenclatures, including neutral endopeptidase or enkephalinase (EC 3.4.24.11) [9–14], endothelin-converting enzymes—ECE1 and ECE2 (EC 3.4.24.71) [15–19]—Kell blood group antigens [20,21], phosphate-regulating neutral endopeptidase on the X chromosome (PEX or PHEX) [22,23], X-converting enzymes (XCEs) [24,25], cluster of differentiation 10 (CD10), membrane metalloendopeptidase (MME), and common acute lymphoblastic leukemia antigens (CALLAs) [13,26]. They are present in various tissues, including the nervous system, and are therefore considered ubiquitous proteins responsible for the degradation of numerous regulatory peptides, including the $A\beta$ peptide [27] (Figure 1), consequently inhibiting the progression of amyloid plaque formation [28]. The wide range of canonical substrates suggests its involvement in multiple regulatory functions and its potential role in the diseases present in various systems, including the brain and nervous systems [29].

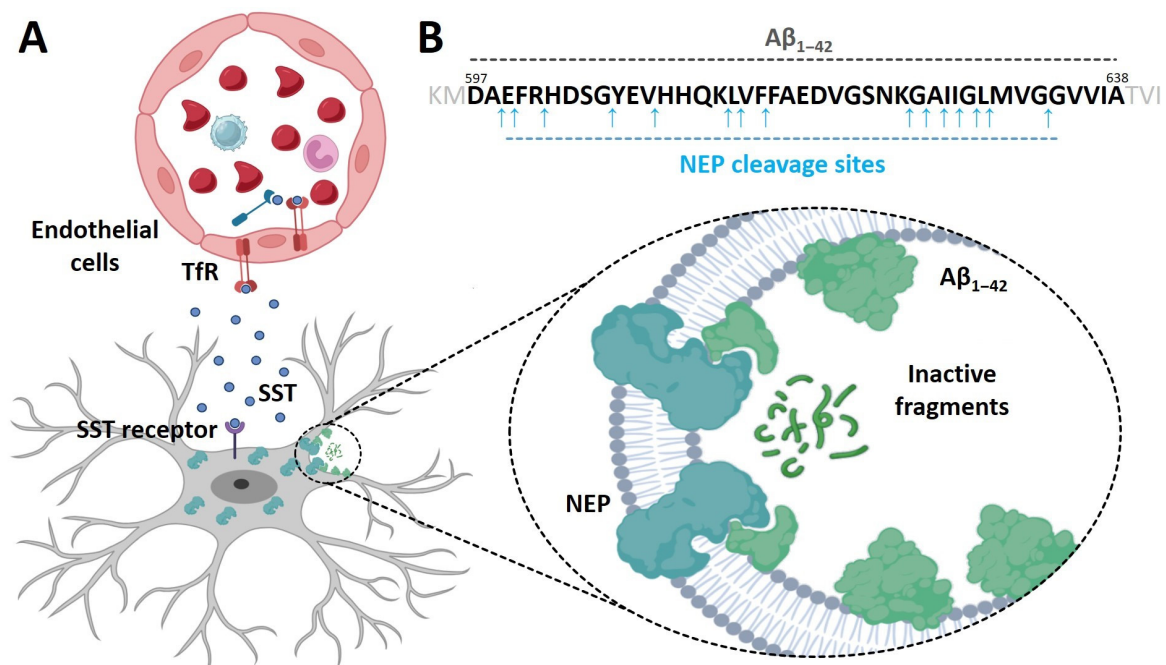


Figure 1. General scheme of the degradation of β -amyloid ($A\beta_{1-42}$) plaques by neprilysin (NEP). (A) Somatostatin-mediated signaling (SST) and induction of NEP expression in nerve cells. (B) Cleavage sites recognized by NEP in $A\beta_{1-42}$ peptides. The amino acid numbers are according to the APP695 isoform, the most highly expressed isoform in neurons—transferrin receptor (TfR).

NEP2(m) features a short N-terminal domain facing the cytoplasmic region, consisting of 27 amino acids, a single transmembrane segment composed of 23 residues, and a substantial C-terminal ectodomain formed by 699 amino acids harboring the catalytic site that extends into the extracellular region [30]. The ectodomain contains a large central cavity corresponding to the catalytic site where the conserved zinc-binding motif HEXXH is located. X stands for any other known amino acid residues. In contrast, two histidine residues are responsible for the coordination of the zinc ion, and glutamate is directly involved in the catalysis process. Structurally, the ectodomain is formed by two alpha-helices, creating a water-filled cleft where the catalytic site is located [31]. Additionally, NEP2(M) is heavily N-glycosylated at the N¹⁴⁵, N²⁸⁵, N²⁹⁴, N³²⁵, and N⁶²⁸ sites [32–35], and the ratio of glycosylation effectively contributes to the range of molecular weights (85–110 kDa) observed in these enzymes in different tissues.

NEP2(m) has been studied extensively under different conditions, including in vitro, in vivo, and in silico [36–42]. Approaches using transgenic NEP2(m) expression analyses have demonstrated decreased neuronal A β deposits in an AD mouse model [43–45]. It was also shown that the overexpression of soluble (active) NEP2(m) in various other studies using animals resulted in significant decreases in the levels of neural A β and improved cognitive performance [46–49]. Additionally, the activity of NEP2(m) in human brain tissue has been shown to increase with normal aging, although an increase was also observed in indicators of AD progression [36]. Therefore, there is much evidence linking the A β accumulation with NEP2(m) activity in induced AD disease, suggesting that this endopeptidase is a promising therapeutic agent capable of minimizing the adverse effects of AD. While it has been documented that NEP2(m) can significantly reduce the A β peptide pool, other neuropeptides are targets of its proteolytic activity, given that it is a promiscuous enzyme [20,50,51]. Thus, high NEP2(m) concentrations can likely lead to imbalances in the necessary neuropeptides in signal pathways that control blood pressure, pain, and other crucial physiological processes.

On the other hand, (-)- α -bisabolol (α -bisabolol) is widely available and dietarily bioavailable. It possesses physicochemical properties that give it lipophilicity [52] and various pharmacological attributes, including anti-inflammatory, antioxidant [53,54], wound healing, antibiotic, antimutagenic, antitumor, gastroprotective, analgesic, and antimicrobial effects [52,55–60] and low toxicity, with its generally recognized as safe (GRAS) status. Recent data suggest that the oral administration of α -bisabolol may provide neuroprotection through decreased neurodegeneration and neuroinflammation, as well as cognitive improvement [57]. In addition, various studies have shown that this substance can significantly reduce the aggregation of A β and act on the cleavage of its fibrillar isoforms [28,61]. α -bisabolol may act by increasing the effectiveness of A β degradation [28,57,62]. This evidence points to an interaction between NEP2(m) and α -bisabolol as a possible mechanism to increase the anti-amyloidogenic effect. Thus, the present study aims to investigate, using computational tools, the interaction between α -bisabolol and NEP2(m), the main A β -degrading enzyme, as a possible anti-amyloidogenic pathway.

2. Materials and Methods

2.1. Domain and Motif Prediction

The amino acid sequence (accession ID Q9JLI3) of murine neprilysin [NEP2(m)] was downloaded in FASTA format from the Universal Protein Resource—UniProt [63]. Then, boundary domains and motif sequences were identified from the amino acid sequence of NEP2(m) using the following servers: Database of Protein Domains, Families and Functional Sites—Prosite [64], Conserved Domains Database and Resources—CDD [65], and Classification of Protein Families—InterPro [66].

2.2. Structural Prediction of the Ectodomain of NEP2(m)

The structural model of the ectodomain portion (Thr⁷⁶–Trp⁷⁶⁵) was predicted using the Modeller program package v.10.0 [67]. For this purpose, experimentally determined

protein structures with similar amino acid sequences were searched using the BLASTp tool with the PSI-BLAST algorithm from the Protein Data Bank [68–70]. This search identified the substrate-free human neprilysin with accession ID 6SH1 as the template [71], which presents a sequence coverage and identity of 92% and 93.8%, respectively. Following this strategy, several models were initially generated, including structural waters and the zinc ion in human neprilysin. Afterward, the produced structures were selected based on the estimated DOPE Score [72], and the top 10 models were chosen for stoichiometry evaluation (steric overlaps, C β deviation parameters, Ramachandran plots, rotamers, and bond angle quality) through the MolProbity Server [73–76]. Finally, the best model was selected and visually inspected with Pymol (Schrödinger).

2.3. Bioactivity Prediction of the α -Bisabolol

The 3D structure of α -bisabolol (CID: 1549992) in PDB format and its file in the SMILES extension were downloaded from the PubChem server (<https://pubchem.ncbi.nlm.nih.gov/>, accessed on 16 February 2024). The SMILES file was then subjected to the Molinspiration virtual screening (www.molinspiration.com, accessed on 16 February 2024) server to evaluate molecular properties and bioactivity scores. The PDB format file was used in the docking and dynamics molecular simulations.

2.4. Prediction of Pockets in NEP2(m) and Docking Calculations

The most favorable hotspot found in leu-enkephalin was determined by both servers: the DogSiteScorer tool [77] and the CASTp server [78]. After determining the most favorable hotspot for interaction, site-directed redocking simulations were conducted in a setup where all the torsional bonds of both α -bisabolol and the side chains of the amino acids found in different experimental structures had the freedom to rotate. Furthermore, all hydrogen polar atoms were added to leu-enkephalin and then parameterized with Gasteiger charges, while the α -bisabolol was prepared with the addition of Kollman charges, as according to previous studies [79,80].

Docking simulations involving the substrate NEP2(m), i.e., leu-enkephalin (Tyr-Gly-Gly-Phe-Leu, seen in Figure 2A), a typical substrate for neprilysin, and α -bisabolol (seen in Figure 2B) were conducted using the AutoDock Vina software version 1.2.0 [81]. For this purpose, the structure of leu-enkephalin was parameterized using the BIOVIA Discovery Studio Package, while α -bisabolol (CID: 1549992) was obtained from PubChem (<https://pubchem.ncbi.nlm.nih.gov/>, accessed on 20 August 2023). To confirm the accuracy of the molecular docking investigations, blind docking simulations were performed in a setup where all the torsional bonds of α -bisabolol had the freedom to rotate, while the amino acids found in different experimental structures (add IDs) were kept rigid. The simulation was performed under the following conditions: number of conformations = 20, exhaustiveness = 8, and seed = 2009. The dimensions of the boxes in all cases were X = 20 Å, Y = 20 Å, and Z = 20 Å.

For all calculations, the ten top-ranked generations based on the predicted binding affinity (in kilocalories per mole) were visually analyzed, and the best results were selected based on structural comparisons made with the experimental structures and their binding profiles. AutoDock Vina was validated for the presented purpose through redocking calculations with different crystal structures, and the results of which were analyzed by the root mean square deviation (RMSD) of the atomic positions between the experimentally determined and calculated ligands through the RMSD calculator tool of the software Visual Molecular Dynamics 1.9 [82].

3. Results

3.1. Prediction of the Domains and Motifs of the Ectodomain of NEP2(m)

The CDD-based prediction data showed that the ectodomain of NEP2(m) is a member belonging to the conserved protein domain of the M13 family of metallopeptidases, which includes neprilysin (neutral endopeptidase, NEP, enkephalinase, CD10, CALLA, EC 3.4.24.11), endothelin-converting enzyme I (ECE-1, EC 3.4.24.71), erythrocyte surface antigen KELL (ECE-3), phosphate-regulating gene on the X chromosome (PHEX), soluble secreted endopeptidase (SEP), and damage-induced neuronal endopeptidase (DINE)/X-converting enzyme (XCE). In addition, the analysis of the CDD-based annotation showed predictions with the following confidence indices: an *E*-value of 0⁰⁰, a bit score of 787.33, and an interval (96 to 763 amino acid residues). The predictions from the Prosite and InterPro servers agree with the data obtained from the CDD server.

3.2. Structural Analysis of the Ectodomain of NEP2(m)

The final NEP2(m) model was analyzed for its stereochemical properties, revealing that 99.8% of amino acid residues were positioned within allowed regions (96% in the favored areas) of the Ramachandran plot. The overall predicted structure of NEP2(m) closely resembles that of other neprilysin and neprilysin-like proteins, displaying a typical α -helical ellipsoid shape consisting of subdomains 1 and 2 connected by a linker region (Figure 3A). The catalytic site is within subdomain 1, positioned over a spacious cavity (approximately 6.278 Å³) formed by both subdomains and the linker region. This catalytic site houses a zinc-binding site with a conserved zinc metalloprotease motif HEXXH, which includes residues His⁵²⁴ and His⁵²⁸ for ion binding (along with residue Glu⁵⁸⁷), as well as the catalytic residue Glu⁵²⁵ (Figure 3B). The zinc atom acts as a cofactor for catalysis, coordinated by well-described ionic interactions with the residues mentioned above, establishing essential contacts directly with the substrate.

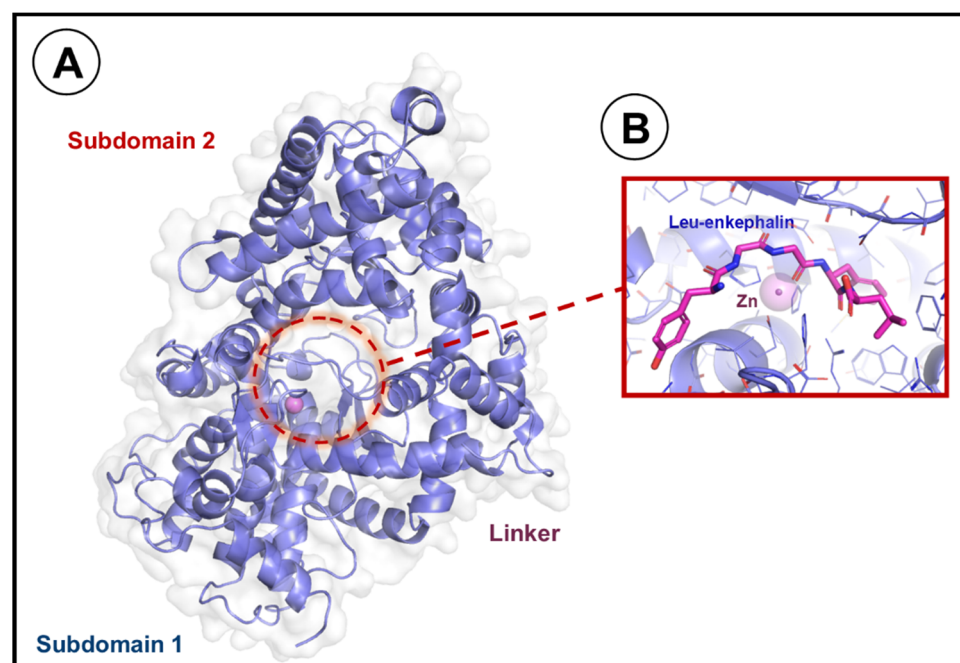


Figure 3. The general structure of NEP2(m). (A) The predicted structure is presented as a light-purple cartoon covered by a transparent white surface. (B) Catalytic site of NEP2(m). The protein is depicted as light-purple lines and a cartoon, while the leu-enkephalin peptide is shown as pink sticks. The zinc ion is represented as a purple sphere in both panels.

3.3. Ligand Bioactivity Prediction

The *in silico* predictions of α -bisabolol bioactivity using Molinspiration virtual screening yielded a score of -0.38 , indicating that this molecule weakly inhibited proteases, particularly metalloproteases belonging to the M13 family. Additionally, the analysis returned a score of -0.06 , suggesting that the ligand bound weakly to G protein-coupled receptors (GPCRs). α -bisabolol also exhibited reduced inhibitory activity against kinases, with a score of -0.78 . The predicted bioactivity of the entire ligand was determined by adding the bioactivity scores of each fragment (usually ranging from -3 to 3). Fragments with lower activity scores were more likely to be inactive.

3.4. Molecular Docking Studies and Molecular Dynamics

The docking calculations for leu-enkephalin were validated through a redocking performed with the crystal structure of human neprilysin (NEP(h)) determined in the presence of the inhibitor omopatriilat (Omlat) (PDB ID 6SUK), which had a chemical structure similar to the analyzed peptide. The RMSD between the best calculated conformation for omopatriilat (Omlat) and its crystal structure was 0.7 , confirming the reliability of AutoDock Vina for predicting binding conformations in similar systems.

The results obtained from the docking calculations with leu-enkephalin were evaluated based on a comparative analysis with the crystal complex between NEP(h) and Omlat, which was associated with the energy assessment of these results through the Prodigy web-server and led us to a promising conformation. This analysis suggests that leu-enkephalin interacts with NEP2(m) in a highly conservative manner when compared to the crystallized ligand (Figure 4A), forming direct contacts with the zinc ion and numerous surrounding amino acids, including several hydrophobic contacts with residues Phe⁵⁰, Ala⁴⁸⁴, Phe⁴⁸⁵, Phe⁵⁰⁴, Val⁵²¹, Trp⁶³⁴, and Val⁶⁵¹, as well as polar contacts with His²³⁷, His²⁵⁸, Asn⁴⁸³, His⁶⁵², and Arg⁶⁵⁸, among others, achieving a calculated binding energy of -6.42 Kcal/mol (Figure 5A and Table 1).

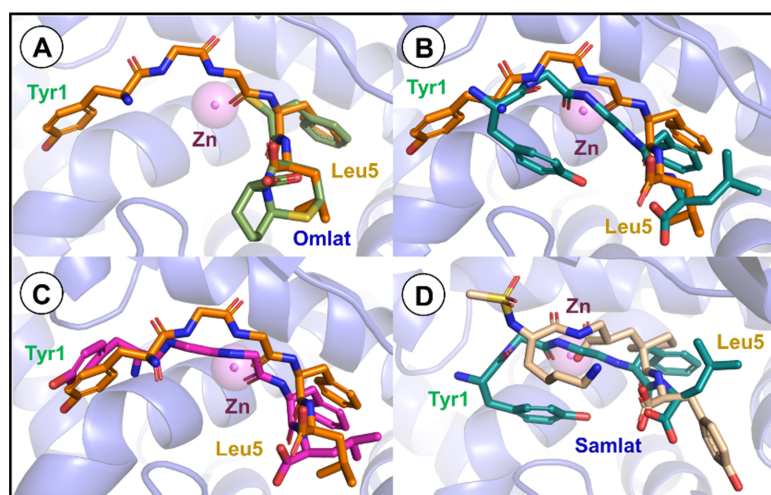


Figure 4. Structural comparison of the binding modes of different ligands in the NEP(h) and NEP2(m) catalytic sites. The protein backbone and the zinc ion are represented as a light-purple transparent cartoon and a transparent purple sphere, respectively. (A) The best docking pose for leu-enkephalin is shown as orange sticks, while the omopatriilat crystal structure is presented as light-green sticks. (B) The best docking pose for leu-enkephalin and its final conformation after 20 ns MD without α -bisabolol are represented as orange and cyan sticks, respectively. (C) The best docking pose for leu-enkephalin and its final conformation after 20 ns MD in the presence of α -bisabolol are represented as orange and pink sticks, respectively. (D) The final conformation of leu-enkephalin after 20 ns MD in the absence of α -bisabolol and the crystal structure of sampatriilat are shown as cyan and dark-yellow sticks, respectively.

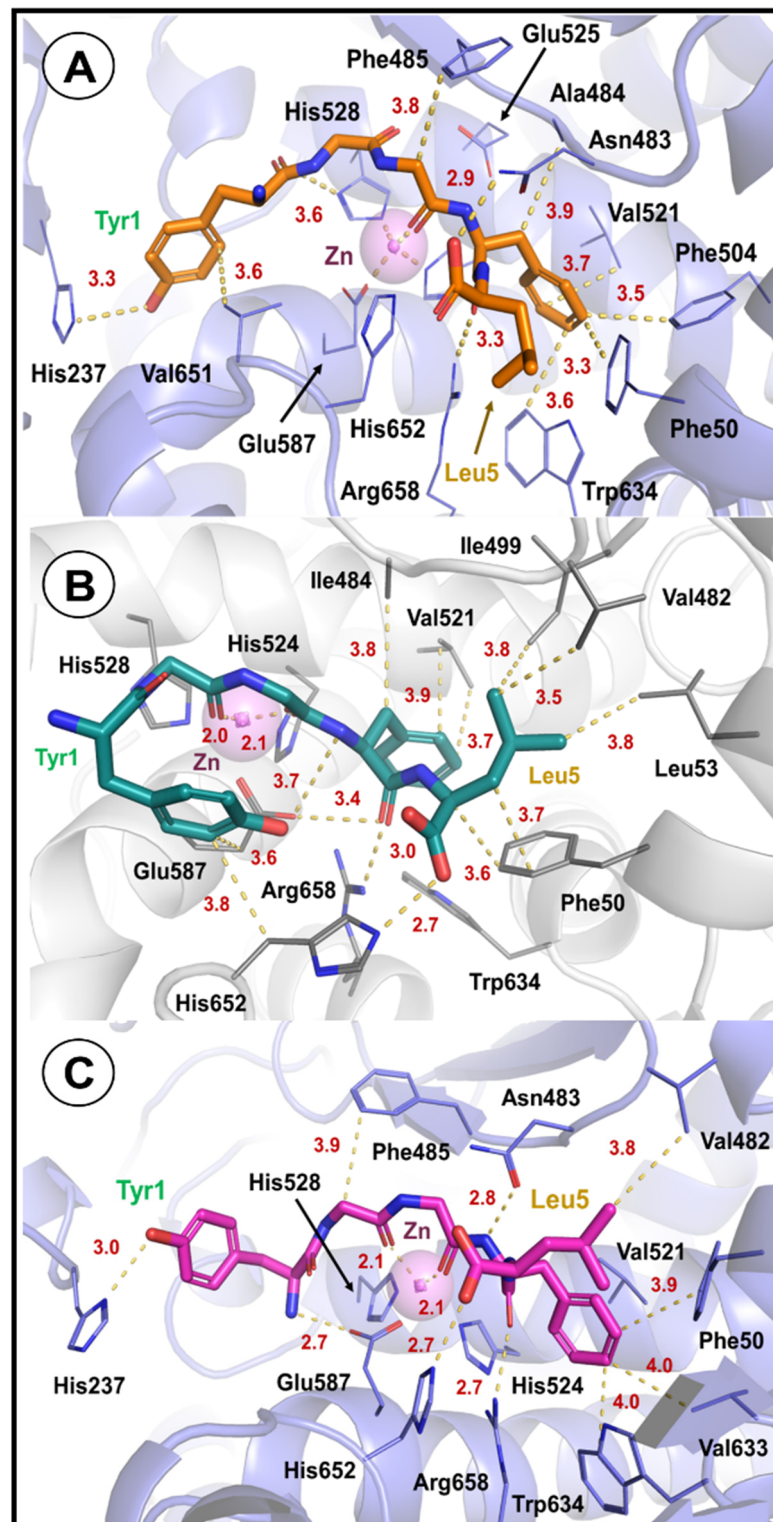


Figure 5. Leu-enkephalin binding analysis regarding NEP2(m). (A) The best docking pose for leu-enkephalin, represented as orange sticks. (B) Final conformation of leu-enkephalin after 20 ns MD in the absence of α -bisabolol, represented as cyan sticks. (C) Final conformation of leu-enkephalin after 20 ns MD in the presence of α -bisabolol, represented as pink sticks. The protein backbone and the zinc ion are represented as a light-purple transparent cartoon and a transparent purple sphere, respectively. NEP2(m) binding residues and molecular interactions are represented by light-purple lines and yellow dashes. For clarity, a few interactions and binding residues are omitted.

Table 1. Docking calculations determine residues and bonds involved in leu-enkephalin coordination.

Neprilysin		Leu-Enkephalin		Bond Properties	
Residue	Atom	Residue	Atom	Type of Interaction	Distance (Å)
His ²³⁷	NE2	Tyr ¹	OH	H-bond	3.3
His ²⁵⁸	ND1	Tyr ¹	O	Van der Waals	3.6
Ser ⁵³⁸	O	Tyr ¹	OH	H-bond	3.0
Val ⁶⁵¹	CG2	Tyr ¹	CD1	Hydrophobic	3.6
Glu ⁵²⁵	OE1	Gly ²	O	H-bond	3.2
Phe ⁴⁸⁵	CD2	Gly ³	CA	Hydrophobic	3.8
Glu ⁵⁸⁷	OE2	Gly ³	O	H-bond	3.5
ZN	ZN	Gly ³	O	Metal coordination	2.0
Phe ⁵⁰	CZ	Phe ⁴	CE1	Hydrophobic	3.3
Asn ⁴⁸³	OD1	Phe ⁴	N	H-bond	3.3
Ala ⁴⁸⁴	CB	Phe ⁴	CB	Hydrophobic	3.9
Phe ⁵⁰⁴	CE1	Phe ⁴	CE1	Hydrophobic	3.5
Val ⁵²¹	CG2	Phe ⁴	CE2	Hydrophobic	3.7
Glu ⁵⁸⁷	OE2	Phe ⁴	N	Van der Waals	3.6
Trp ⁶³⁴	CZ2	Phe ⁴	CZ	Hydrophobic	3.6
His ⁶⁵²	NE2	Phe ⁴	O	H-bond	3.2
Arg ⁶⁵⁸	NH1	Phe ⁴	O	H-bond	3.0
Phe ⁵⁰	CG	Leu ⁵	CG	Hydrophobic	3.6
Asn ⁴⁸³	OD1	Leu ⁵	N	H-bond	3.0
Asn ⁴⁸³	ND2	Leu ⁵	OXT	Hydrophobic	2.9
His ⁶⁵²	ND1	Leu ⁵	O	Van der Waals	3.6

Additionally, the fact that leu-enkephalin is cleaved by NEP2(m) at the Gly³-Phe⁴ bond is in perfect accordance with the calculations since the OE2 group from the catalytic residue Glu⁵²⁵ is disposed 3.6 Å from the peptide bond mentioned above. A previous description involving the complex between NEP(h) and the inhibitor *N*-(3-Phenyl-2-sulfanylpropanoyl) phenylalanyl-alanine (PDB ID 1R1J) reported a distance of 3.3 Å for this bond, corroborating the calculated conformation. Nevertheless, since the interaction between the enzyme and the substrate was a dynamic process, MD simulations were performed with the aim of better understanding the behavior of leu-enkephalin at the catalytic site in the absence and presence of α -bisabolol.

We observed that leu-enkephalin exhibited a generally stable behavior at the catalytic site in the absence of α -bisabolol during the 20 ns of MD simulations, as observed by its RMSD (Figures 6A and 7B). However, its terminal residues (Tyr¹ and Leu⁵) underwent a significant rearrangement throughout the simulation, allowing leu-enkephalin to assume a folded conformation similar to another crystallized inhibitor [NEP(h)], sampatri-lat (Samlat), which had a more prolonged and more extended structure compared to Omlat (Figure 4D). Among the 11 polar contacts (including seven hydrogen bonds) predicted by docking calculations, only two were sustained along MD, established with residues Arg⁶⁵⁸ and His⁶⁵². However, a new hydrogen bond was detected after the simulations between Tyr¹ and Glu⁵⁸⁷ (Tables 1 and 2). This rearrangement was associated with the observed flexibility of the segment Val⁴⁸¹-Pro⁴⁸⁸, which directly interacted with the peptide (Figure 6C). Nevertheless, this adjusted conformation was quickly achieved and stabilized by the peptide (Figure 5B and Table 2), which presented a calculated binding energy of -6.59 Kcal/mol at the final frame after MD. Such a structural rearrangement possibly influenced the effectiveness and speed of the substrate cleavage as the precise alignment of chemical groups was crucial in the catalytic process.

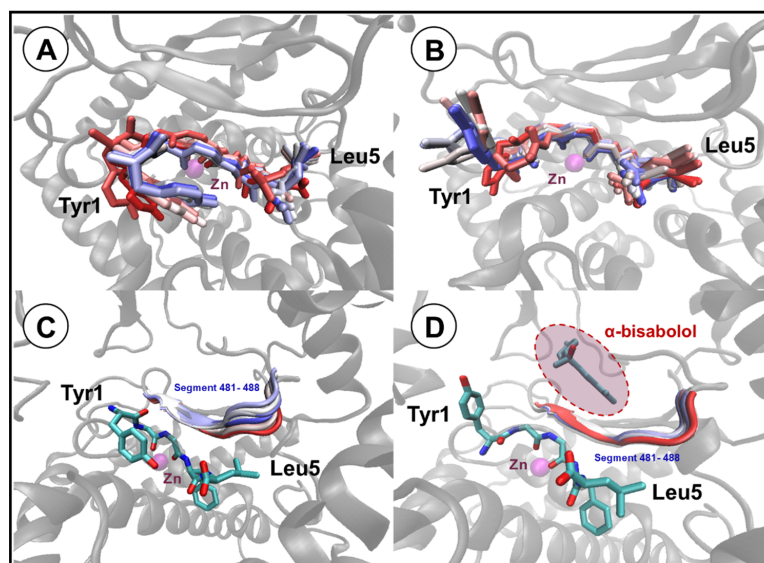


Figure 6. Molecular dynamics analysis of leu-enkephalin and NEP2(m). (A) Structural oscillation of leu-enkephalin along 20 ns MD without α -bisabolol. (B) Structural oscillation of leu-enkephalin along 20 ns MD in the presence of α -bisabolol. (C) Structural oscillation of segment Val⁴⁸¹-Pro⁴⁸⁸ along 20 ns MD without α -bisabolol. (D) Structural oscillation of segment Val⁴⁸¹-Pro⁴⁸⁸ along 20 ns MD in the presence of α -bisabolol. The highlighted structural oscillations are presented through time by color transition (red—initial conformation, white—conformation around 10 ns, blue—final conformation at 20 ns). The protein backbone is represented as a light-gray transparent cartoon, while leu-enkephalin and α -bisabolol are represented as colored sticks, and segment Val⁴⁸¹-Pro⁴⁸⁸ is represented as a colored cartoon.

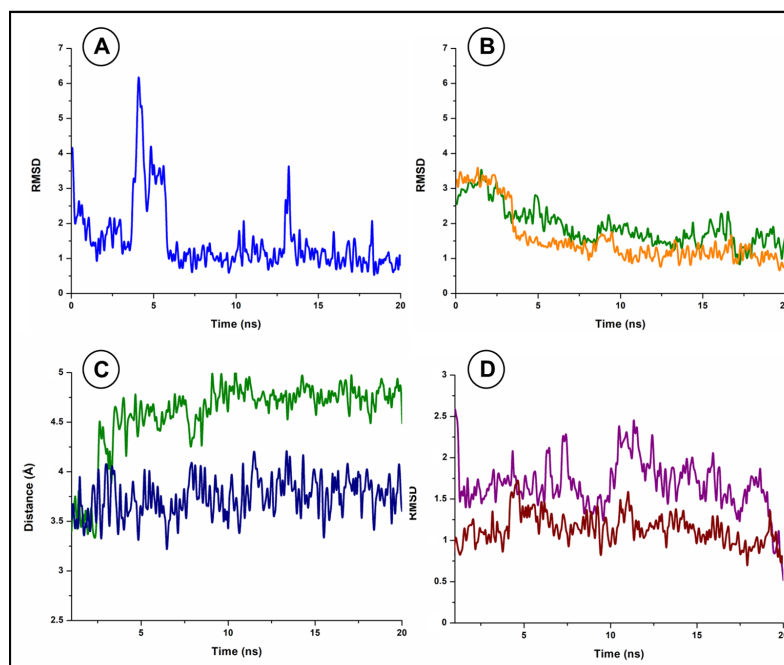


Figure 7. RMSD variation along molecular dynamics simulations. (A) α -bisabolol RMSD curve (blue). (B) Leu-enkephalin RMSD curves in the absence (orange) and presence (green) of α -bisabolol. (C) Bond distance variation between the atoms OE2 from the catalytic residue Glu⁵²⁵ and N from residue Phe⁴ (van der Waals) in leu-enkephalin in the absence (green) and presence (blue) of α -bisabolol. (D) Segment Val⁴⁸¹-Pro⁴⁸⁸ RMSD curves in the absence (purple) and presence (wine) of α -bisabolol.

Table 2. Docking calculations and molecular dynamics determine residues and bonds involved in leu-enkephalin coordination without α -bisabolol.

Neprilysin		Leu-Enkephalin		Bond Properties	
Residue	Atom	Residue	Atom	Type of Interaction	Distance (Å)
Glu ⁵⁸⁷	CG	Tyr ¹	CE1	Hydrophobic	3.6
Glu ⁵⁸⁷	OE2	Tyr ¹	OH	H-bond	2.8
His ⁶⁵²	CB	Tyr ¹	CE1	Hydrophobic	3.8
ZN	ZN	Gly ²	O	Metal coordination	2.0
ZN	ZN	Gly ³	O	Metal coordination	2.1
Ala ⁴⁸⁴	CB	Phe ⁴	CB	Hydrophobic	3.8
Val ⁵²¹	CG2	Phe ⁴	CE1	Hydrophobic	3.7
His ⁵²⁴	CD2	Phe ⁴	CD2	Hydrophobic	3.6
Glu ⁵⁸⁷	OE2	Phe ⁴	O	H-bond	3.4
Arg ⁶⁵⁸	NH1	Phe ⁴	O	H-bond	3.0
Phe ⁵⁰	CE2	Leu ⁵	CA	Hydrophobic	3.6
Leu ⁵³	CD2	Leu ⁵	CD2	Hydrophobic	3.8
Val ⁴⁸²	CG1	Leu ⁵	CD1	Hydrophobic	3.5
Ile ⁴⁹⁹	CD	Leu ⁵	CD1	Hydrophobic	3.8
His ⁶⁵²	NE2	Leu ⁵	OT2	H-bond	2.7

To understand this effect, the length variation between the catalytic residue Glu⁵²⁵ and the peptide bond that linked residues Gly³ and Phe⁴ in leu-enkephalin was analyzed (Figure 6C). It was observed that the distance between these groups significantly increased after two ns of simulation. From 5 ns until the end of the simulation, it oscillated between 4.5 and 5 Å (Figure 7C). This was a far more considerable distance than observed in the crystal structures of neprilysin from different organisms in a complex with substrates with a peptide bond at this very position. For instance, in the case of NEP(h) complexed with the inhibitor *N*-(3-Phenyl-2-sulfanylpropanoyl) phenylalanyl-alanine (PDB ID 1R1J), the mentioned distance was 3.3 Å. Therefore, this computational evidence pointed toward a lower stability of longer peptides at the NEP2(m) catalytic site, which would have directly affected the rate of substrate processing.

Regarding the calculations with α -Bisabolol, blind docking primarily identified anchoring sites over the catalytic site of NEP2(m) and its vicinity, strengthening the hypothesis that this molecule can modulate neprilysin activity. As previously described, the reliability of AutoDock Vina for this purpose was validated through redocking calculations, this time involving the crystal structure of the complex between tobacco 5-epi-aristolochene synthase and the sesquiterpene germacrene A, which is a compound from the same group as α -bisabolol. The RMSD between the best calculated conformation for germacrene A and its crystal structure was 0.05, strongly confirming the reliability of AutoDock Vina.

Afterward, the search area for the docking calculations was delimited to the vicinities of the catalytic site, allowing the identification of a promising conformation in which α -Bisabolol interacted with NEP2(m) and leu-enkephalin. However, during MD simulations, an exciting accommodation of α -bisabolol was observed, as shown by its RMSD (Figure 7A), which quickly shifted its interacting site (initially over leu-enkephalin) to a small cavity located over segment Val⁴⁸¹-Pro⁴⁸⁸, where it remained stable (Figure 6D). This cavity was not identified during the docking calculations due to its unavailability as the initial structure of NEP2(m) presented a closed conformation that opened and became accessible during MD simulations.

The α -bisabolol binding site presents a volume of 121.8 Å³ and a surface area of 223.7 Å², composed mainly of residues Trp¹⁴⁹, Ile⁴⁷⁶, Ile⁴⁷⁷, Asn⁴⁸³, Phe⁴⁸⁵, and Arg⁴⁹⁰, which anchor the ligand solely through hydrophobic interactions, achieving at its final frame after the MD-calculated binding energy of -7.16 Kcal/mol (Figure 8 and Table 3). This high hydrophobicity is likely the reason why the binding site remains closed in the

absence of an appropriate ligand, a fact already described for different lipases that shift their conformations in the presence of detergents towards an open form, permitting hydrophobic ligands to access the active site through the interfacial activation of the enzyme.

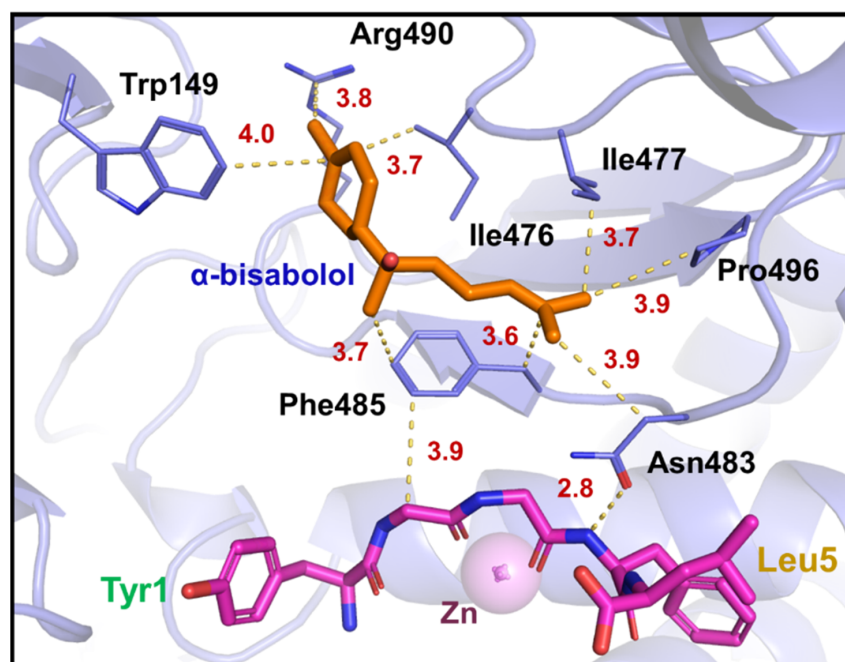


Figure 8. α -bisabolol binding site. Leu-enkephalin and α -bisabolol are represented as pink and orange sticks, respectively. The protein backbone and interacting residues from NEP2(m) are shown as a light-purple cartoon and lines, while the zinc ion is represented as a purple transparent sphere, respectively. Molecular interactions are presented as yellow dashes. For clarity, a few interactions and binding residues are omitted.

Table 3. Docking calculations and molecular dynamics determine residues and bonds involved in α -bisabolol coordination.

Neprilysin		α -Bisabolol		Bond Properties	
Residue	Atom	Atom	Type of Interaction	Distance (Å)	
Trp ¹⁴⁹	CH2	C13	Hydrophobic	4.1	
Ile ⁴⁷⁶	CG2	C13	Hydrophobic	3.7	
Ile ⁴⁷⁶	CB	C13	Hydrophobic	3.9	
Ile ⁴⁷⁶	O	H14	Van der Waals	2.6	
Ile ⁴⁷⁷	CB	C12	Hydrophobic	4.0	
Asn ⁴⁸³	ND2	H11	Van der Waals	3.0	
Phe ⁴⁸⁵	Centroid	C7	π -alkyl	4.1	
Arg ⁴⁹⁰	NH2	H6	Van der Waals	3.0	
Pro ⁴⁹⁶	CG	C4	Hydrophobic	4.1	

The MD simulations demonstrate that the presence of α -bisabolol stabilizes the segment Val⁴⁸¹-Pro⁴⁸⁸, as observed by its structural variation and RMSD (Figures 6D and 7D). This segment stabilization is also reflected over leu-enkephalin since it establishes significant contact with this segment (Figures 5C and 6B and Table 4). Consequently, the coordinates obtained for leu-enkephalin after MD in the presence of α -bisabolol closely resemble the result of the docking calculations, presenting a higher calculated binding energy of -6.99 Kcal/mol (Figure 4B,C). This sesquiterpene allowed the maintenance of 7 from the 11 polar contacts predicted by the docking calculations beyond establishing two new hydrogen bonds between Tyr¹ and Glu⁵⁸⁷ (Tables 1 and 4).

Table 4. Residues and bonds involved in leu-enkephalin coordination in the presence of α -bisabolol determined by docking calculations and molecular dynamics.

Neprilysin		Leu-Enkephalin		Bond Properties	
Residue	Atom	Residue	Atom	Type of Interaction	Distance (Å)
His ²³⁷	ND1	Tyr ¹	OH	H-bond	3.0
Glu ⁵⁸⁷	OE2	Tyr ¹	N	H-bond	2.7
Glu ⁵⁸⁷	OE2	Tyr ¹	O	H-bond	3.1
Phe ⁴⁸⁵	CE1	Gly ²	CA	Hydrophobic	3.9
ZN	ZN	Gly ²	O	Metal coordination	2.1
ZN	ZN	Gly ³	O	Metal coordination	2.1
Asn ⁴⁸³	OD1	Phe ⁴	N	H-bond	2.8
Glu ⁵²⁵	OE2	Phe ⁴	N	Van der Waals	4.0
His ⁵²⁴	CE1	Phe ⁴	CD2	Hydrophobic	3.9
Val ⁵²¹	CG2	Phe ⁴	CZ	Hydrophobic	3.9
Trp ⁶³⁴	CE2	Phe ⁴	CZ	Hydrophobic	4.0
Val ⁶³³	CG2	Phe ⁴	CZ	Hydrophobic	4.0
Phe ⁵⁰	CZ	Phe ⁴	CE1	Hydrophobic	3.9
Arg ⁶⁵⁴	NH1	Phe ⁴	O	H-bond	2.8
Asn ⁴⁸³	OD1	Leu ⁵	N	H-bond	2.9
Asn ⁴⁸³	ND2	Leu ⁵	OT2	Van der Waals	4.0
His ⁶⁵²	NE2	Leu ⁵	OT1	H-bond	2.7
Val ⁴⁸²	CG1	Leu ⁵	CD1	Hydrophobic	3.8
Phe ⁵⁰	CG	Leu ⁵	CD2	Hydrophobic	3.9

Although no direct contact between α -bisabolol and the peptide are observed, there are residues in NEP2(m) at the segment Val⁴⁸¹-Pro⁴⁸⁸ that interact with both, playing an essential role in the stabilization of the peptide, such as Asn⁴⁸³ and Phe⁴⁸⁵. While Phe⁴⁸⁵ performs hydrophobic contact with α -bisabolol and the peptide, Asn⁴⁸³ interacts at a short range (2.8 Å) with the nitrogen group from the residue Phe⁴ in leu-enkephalin through a hydrogen bond, which is precisely the peptide bond cleaved by NEP2(m) (Figure 8). The distance variation between the catalytic residue Glu⁵²⁵ and the Gly³-Phe⁴ peptide bond in leu-enkephalin is considerably lower in the presence of α -bisabolol, remaining in the range between 3.5 and 4 Å throughout the entire simulation (Figure 7C). This fact can be associated with the described stabilizing effects of α -bisabolol, which corroborate its potential impact on the positive modulation of NEP2(m).

4. Discussion

Pockets and cavities found in receptors often correspond to the active sites responsible for biological processes. Therefore, comprehending their physicochemical properties is fundamental [79]. Thus, the predictions of binding hotspots were determined in the catalytic pocket of NEP2(m), a member of the M13 family of peptidases, which is a zinc-dependent type II integral membrane metallopeptidase [87]. For this purpose, small organic molecules were employed as probes. The integration of the results revealed the existence of only one hotspot in NEP2(m), which served as a region that could contribute to the ligand binding free energy (Gibbs free energy). The NEP2(m) is formed by 749 amino acid residues. Its structure consists of three main parts: (I) a short *N*-terminal cytoplasmic domain, (II) a single transmembrane helix, and (III) a *C*-terminal extracellular domain. The extracellular domain is bound to a zinc atom at its active site, serving as a cofactor for catalyzing substrates [16]. Among the substrates of NEP2(m) are hydrophobic residues found in peptides (size \leq 3 kDa), with a preference for sites containing phenylalanine and leucine [88,89]. Additionally, the extracellular domain also features two helical structures that create a cleft housing the catalytic site of the enzyme [32].

Neprilysin is widely spread over human tissues (Figure 9) and is crucial in the processing and breakdown of various peptides, including vasoactive peptides involved in diuresis and natriuresis. The most notable peptides include natriuretic peptides (NPs), angiotensin I (Ang I), adrenomedullin (ADM), bradykinin (BK), neurokinin A, neuropeptide Y, substance P, and endothelin [90–95]. Additionally, neprilysin also antagonizes neurological processes, pain, inflammation, mitogenesis, angiogenesis, digestion, and other functions [96,97]. On the other hand, previous studies using α -bisabolol suggest that it has the potential to reduce beta-amyloid plaques, thus providing a possibility of treatment for Alzheimer's disease [98,99]. These findings emphasize the neuroprotective role of α -bisabolol against A β -mediated neurotoxicity, attributed to its inhibition of A β fibrillization and a possible interaction with neprilysin.

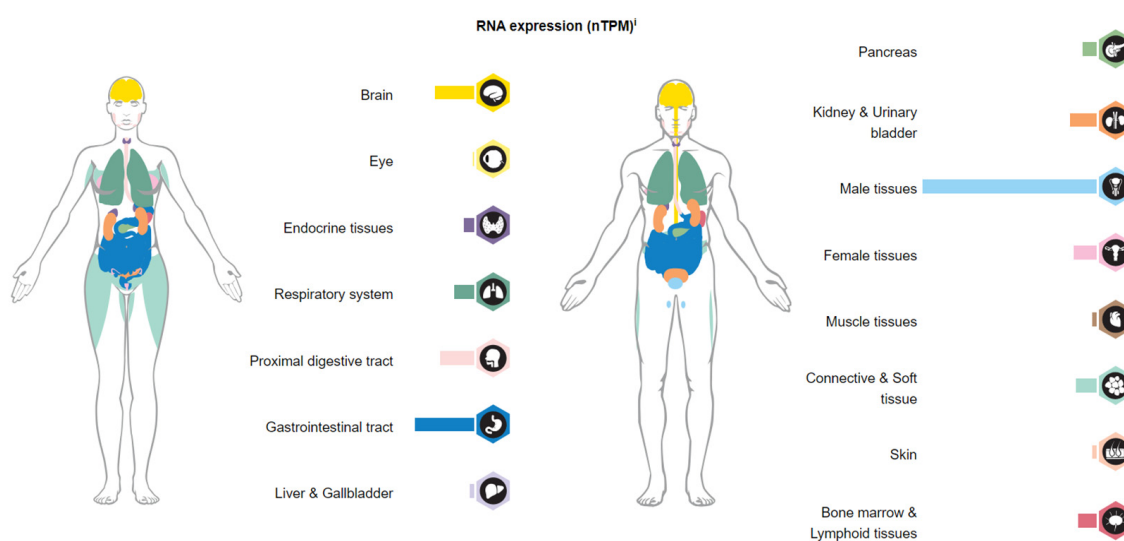


Figure 9. Human tissues and organs in which NEP2(m) mRNA are expressed. The right side of the image shows tissues and organs where the expression of mRNA coding for NEP2(m) occurs in men, while the left side shows tissues and organs where the expression of mRNA coding for NEP2(m) occurs in women. Data were extracted from the electronic source/address <https://www.proteinatlas.org/>, accessed on 5 April 2024.

Furthermore, the *in silico* prediction of the α -bisabolol ligand, based on Molinspiration virtual screening, indicated a low bioactivity score (-0.38) against multiple proteases, including metalloproteases such as NEP2(m). Bioactivity prediction performed by the Molinspiration virtual screening is based on the sum of the bioactivity scores of all individual fragments of the molecule investigated, typically ranging from -3 to 3 . Corroborating with our predictions, a recent study indicated that α -bisabolol is capable of disrupting the proper functional processes of metalloproteases [56]. The weak inhibitory capacity of α -bisabolol on metalloproteases may be closely associated with the size of specific peptide substrates or the presence of poorly competitive or non-competitive ones. Thus, the presence of α -bisabolol in the catalytic site can prevent the adequate accommodation of larger peptide substrates and therefore induce weak inhibition as predicted for this class of proteases. However, the presence of α -bisabolol in the catalytic site of NEP2(m) appears to facilitate the better accommodation of small peptide substrates such as leu-enkephalin.

This was demonstrated by the molecular dynamics analysis of α -bisabolol, leu-enkephalin, and NEP2(m), as illustrated in Figure 6B,D. Our data suggest that α -bisabolol induces greater stability in the segment Val⁴⁸¹-Pro⁴⁸⁸ of NEP2(m), creating a more favorable environment for interaction with the peptide leu-enkephalin. It is worth mentioning that NEP2(m) presents high affinity for hydrophobic peptides (≤ 3 kDa), especially those containing phenylalanine and leucine [100,101]. Many small molecules, including solvent molecules, substrate molecules, and cofactors, can play crucial roles in enzyme catalysis,

influencing the speed and efficiency of specific biochemical reactions, which depend inherently on the dynamic nature of folded structures [102]. Generally, structures can give rise to an ensemble of interconverting conformations (sub-states) driven specifically by thermodynamic fluctuations [103–105], as illustrated in Figure 6A,C.

The physicochemical analysis of NEP2(m) based on the Ramachandran plot (omitted data) reveals that 99.8% of amino acid residues (φ/ψ pairs) are placed within the allowed regions, with 96% falling into the favored areas. These results suggest high-quality torsions and angles for each specific amino acid in the model generated for NEP2(m). It was initially proposed that more than 90% of the φ/ψ pairs should be located in the most favored regions of the plots [106]. However, these regions were later redefined, and the recent estimate suggests that over 98% of the angles should be found within them [73–76]. In this way, all thermodynamic fluctuations observed in the segment Val⁴⁸¹-Pro⁴⁸⁸ of NEP2(m) are likely to occur when devoid of the α -bisabolol ligand. In addition, the induced fit enzymatic model suggests that binding with a specific ligand, such as α -bisabolol, can trigger structural and conformational changes compared to unbound structures. Therefore, the presence of α -bisabolol seems to make the enzymatic reaction of NEP2(m) more specifically about leu-enkephalin. On the other hand, the binding of leu-enkephalin without the presence of α -bisabolol seems to involve the exploration of the conformational space of NEP2(m) and results in a range of reactive possibilities over microsecond to millisecond time scales and longer.

Given the above, this study suggests that α -bisabolol can inhibit A β peptide aggregation in the cerebral cortex region of the brain, thus presenting a promising therapeutic strategy against Alzheimer's disease. Not far from our findings, some studies on α -bisabolol have demonstrated that this compound could have advantageous therapeutic off-target effects [28,56,62,107]. This is in line with its common use in the cosmetic industry, where it is produced for various skin care products, personal hygiene products, and aromatherapy.

5. Conclusions

Here, we present computational evidence supporting the effect of α -bisabolol on the stabilization of leu-enkephalin at the catalytic site of NEP2(m), which can be linked to a positive modulation of the enzyme activity. This effect is achieved through the stabilization of the Val⁴⁸¹-Pro⁴⁸⁸ segment in NEP2(m) by the binding of α -bisabolol, significantly reducing the distance between the catalytic residue Glu⁵²⁵ and the peptide bond Gly³-Phe⁴ in leu-enkephalin, likely enhancing enzyme processivity. As neprilysin has been shown to act as an A β -degrading agent, there have been increasing efforts to develop and discover new promising molecules to improve this capability. However, the findings here underscore the significance of the well-known compound as a promising drug for treating Alzheimer's disease, validating historical knowledge and providing a new avenue for drug design.

Author Contributions: Conceptualization, J.E.R.M., F.S.L.V.-F. and D.d.S.d.A.; methodology, J.E.R.M., J.E.d.C.F., F.S.L.V.-F. and D.d.S.d.A.; validation, J.E.R.M., J.E.d.C.F., F.S.L.V.-F. and D.d.S.d.A.; formal analysis, V.M.C., J.E.d.C.F. and B.L.d.S.; investigation, J.E.R.M., F.S.L.V.-F., D.d.S.d.A. and V.M.C.; writing—original draft preparation, J.E.R.M., J.E.d.C.F., F.S.L.V.-F. and D.d.S.d.A.; writing—review and editing, V.M.C., J.E.d.C.F. and B.L.d.S.; visualization, V.M.C. and J.E.d.C.F.; supervision, B.L.d.S. All authors have read and agreed to the published version of the manuscript.

Funding: This research received no external funding.

Data Availability Statement: Data are contained within the article.

Acknowledgments: We acknowledge the Superior Institute of Biomedical Sciences—State University of Ceará, Fortaleza, CE, Brazil; the Dean of Culture, Federal University of Cariri, Juazeiro do Norte, Fortaleza, Ceará, Brazil; and the Faculty of Philosophy Dom Aureliano Matos, State University of Ceará, Limoeiro do Norte, Ceará, Brazil, for supporting this research, although not financially.

Conflicts of Interest: The authors declare no conflicts of interest.

References

- GBD 2019 Dementia Forecasting Collaborators. Estimation of the Global Prevalence of Dementia in 2019 and Forecasted Prevalence in 2050: An Analysis for the Global Burden of Disease Study 2019. *Lancet Public Health* **2022**, *7*, e105–e125. [[CrossRef](#)] [[PubMed](#)]
- Bovolenta, T.M.; Schumacher-Schuh, A.F.; Santos-Lobato, B.L.d.; Godeiro Júnior, C.d.O.; Silva, D.J.d.; Nicaretta, D.; Barbosa, E.R.; Cardoso, F.E.C.; Della Coletta, M.V.; Braga Neto, P.; et al. Average Annual Cost of Parkinson's Disease in a Brazilian Multiethnic Population. *Park. Relat. Disord.* **2023**, *117*, 105897. [[CrossRef](#)] [[PubMed](#)]
- Bateman, R.J.; Xiong, C.; Benzinger, T.L.S.; Fagan, A.M.; Goate, A.; Fox, N.C.; Marcus, D.S.; Cairns, N.J.; Xie, X.; Blazey, T.M.; et al. Clinical and Biomarker Changes in Dominantly Inherited Alzheimer's Disease. *N. Engl. J. Med.* **2012**, *367*, 795–804. [[CrossRef](#)] [[PubMed](#)]
- Foster, E.M.; Fernandes, M.; Dangla-Valls, A.; Hublitz, P.; Pangalos, M.; Lovestone, S.; Ribe, E.M.; Buckley, N.J. Glycosylated Clusterin Species Facilitate A β Toxicity in Human Neurons. *Sci. Rep.* **2022**, *12*, 18639. [[CrossRef](#)] [[PubMed](#)]
- Ghosh, S.; Ali, R.; Verma, S. A β -Oligomers: A Potential Therapeutic Target for Alzheimer's Disease. *Int. J. Biol. Macromol.* **2023**, *239*, 124231. [[CrossRef](#)] [[PubMed](#)]
- Connor, J.P.; Quinn, S.D.; Schaefer, C. Sticker-and-Spacer Model for Amyloid Beta Condensation and Fibrillation. *Front. Mol. Neurosci.* **2022**, *15*, 962526. [[CrossRef](#)] [[PubMed](#)]
- Schraen-Maschke, S.; Duhamel, A.; Vidal, J.S.; Ramdane, N.; Vaudran, L.; Dussart, C.; Buée, L.; Sablonnière, B.; Delaby, C.; Allinquant, B.; et al. The Free Plasma Amyloid A β 1–42/A β 1–40 Ratio Predicts Conversion to Dementia for Subjects with Mild Cognitive Impairment with Performance Equivalent to That of the Total Plasma A β 1–42/A β 1–40 Ratio. The BALTAZAR Study. *Neurobiol. Dis.* **2024**, *193*, 106459. [[CrossRef](#)] [[PubMed](#)]
- Ju, Y.; Tam, K.Y. Pathological mechanisms and therapeutic strategies for Alzheimer's disease. *Neural Regen. Res.* **2022**, *17*, 543. [[CrossRef](#)] [[PubMed](#)]
- Malfroy, B.; Kuang, W.-J.; Seeburg, P.H.; Mason, A.J.; Schofield, P.R. Molecular Cloning and Amino Acid Sequence of Human Enkephalinase (Neutral endopeptidase). *FEBS Lett.* **1988**, *229*, 206–210. [[CrossRef](#)]
- Malfroy, B.; Schofield, P.R.; Kuang, W.-J.; Seeburg, P.H.; Mason, A.J.; Henzel, W.J. Molecular Cloning and Amino Acid Sequence of Rat Enkephalinase. *Biochem. Biophys. Res. Commun.* **1987**, *144*, 59–66. [[CrossRef](#)]
- Devault, A.; Lazure, C.; Nault, C.; Le Moual, H.; Seidah, N.G.; Chrétien, M.; Kahn, P.; Powell, J.; Mallet, J.; Beaumont, A. Amino Acid Sequence of Rabbit Kidney Neutral Endopeptidase 24.11 (Enkephalinase) Deduced from a Complementary DNA. *EMBO J.* **1987**, *6*, 1317–1322. [[CrossRef](#)] [[PubMed](#)]
- Nakagawa, H.; Saito, Y. Roles of Natriuretic Peptides and the Significance of Neprilysin in Cardiovascular Diseases. *Biology* **2022**, *11*, 1017. [[CrossRef](#)]
- Nalivaeva, N.; Zhuravin, I.; Turner, A. Neprilysin Expression and Functions in Development, Ageing, and Disease. *Mech. Ageing Dev.* **2020**, *192*, 111363. [[CrossRef](#)] [[PubMed](#)]
- Zhi, J.; Yin, L.; Zhang, Z.; Lv, Y.; Wu, F.; Yang, Y.; Zhang, E.; Li, H.; Lu, N.; Zhou, M.; et al. Network Pharmacology-Based Analysis of Jin-Si-Wei on the Treatment of Alzheimer's Disease. *J. Ethnopharmacol.* **2024**, *319*, 117291. [[CrossRef](#)] [[PubMed](#)]
- Xu, D.; Emoto, N.; Giaid, A.; Slaughter, C.; Kaw, S.; deWit, D.; Yanagisawa, M. ECE-1: A Membrane-Bound Metalloprotease That Catalyzes the Proteolytic Activation of Big Endothelin-1. *Cell* **1994**, *78*, 473–485. [[CrossRef](#)] [[PubMed](#)]
- Emoto, N.; Yanagisawa, M. Endothelin-Converting Enzyme-2 Is a Membrane-Bound, Phosphoramidon-Sensitive Metalloprotease with Acidic pH Optimum. *J. Biol. Chem.* **1995**, *270*, 15262–15268. [[CrossRef](#)] [[PubMed](#)]
- Pacheco-Quinto, J.; Clausen, D.; Pérez-González, R.; Peng, H.; Meszaros, A.; Eckman, C.B.; Levy, E.; Eckman, E.A. Intracellular Metalloprotease Activity Controls Intraneuronal A β Aggregation and Limits Secretion of A β via Exosomes. *FASEB J.* **2019**, *33*, 3758–3771. [[CrossRef](#)] [[PubMed](#)]
- Ullah, R.; Lee, E.J. Advances in Amyloid- β Clearance in the Brain and Periphery: Implications for Neurodegenerative Diseases. *Exp. Neurobiol.* **2023**, *32*, 216–246. [[CrossRef](#)]
- Bland, N.D.; Pinney, J.W.; Thomas, J.E.; Turner, A.J.; Isaac, R.E. Bioinformatic Analysis of the Neprilysin (M13) Family of Peptidases Reveals Complex Evolutionary and Functional Relationships. *BMC Evol. Biol.* **2008**, *8*, 16. [[CrossRef](#)]
- Turner, A.J.; Tanzawa, K. Mammalian Membrane Metallopeptidases: NEP, ECE, KELL, and PEX. *FASEB J.* **1997**, *11*, 355–364. [[CrossRef](#)]
- Lee, S.; Zambas, E.D.; Marsh, W.L.; Redman, C.M. Molecular Cloning and Primary Structure of Kell Blood Group Protein. *Proc. Natl. Acad. Sci. USA* **1991**, *88*, 6353–6357. [[CrossRef](#)] [[PubMed](#)]
- Campos, M.; Couture, C.; Hirata, I.Y.; Juliano, M.A.; Loisel, T.P.; Crine, P.; Juliano, L.; Boileau, G.; Carmona, A.K. Human Recombinant Endopeptidase PHEX Has a Strict S1' Specificity for Acidic Residues and Cleaves Peptides Derived from Fibroblast Growth Factor-23 and Matrix Extracellular Phosphoglycoprotein. *Biochem. J.* **2003**, *373*, 271–279. [[CrossRef](#)] [[PubMed](#)]
- Du, L.; Desbarats, M.; Viel, J.; Glorieux, F.H.; Cawthorn, C.; Ecarot, B. cDNA Cloning of the Murine Pex Gene Implicated in X-Linked Hypophosphatemia and Evidence for Expression in Bone. *Genomics* **1996**, *36*, 22–28. [[CrossRef](#)] [[PubMed](#)]
- Ul-Haq, Z.; Iqbal, S.; Moin, S.T. Dynamic Changes in the Secondary Structure of ECE-1 and XCE Account for Their Different Substrate Specificities. *BMC Bioinform.* **2012**, *13*, 285. [[CrossRef](#)] [[PubMed](#)]
- Valdenaire, O.; Richards, J.G.; Faull, R.L.M.; Schweizer, A. XCE, a New Member of the Endothelin-Converting Enzyme and Neutral Endopeptidase Family, Is Preferentially Expressed in the CNS. *Mol. Brain Res.* **1999**, *64*, 211–221. [[CrossRef](#)] [[PubMed](#)]

26. Ramirez, A.K.; Dankel, S.; Cai, W.; Sakaguchi, M.; Kasif, S.; Kahn, C.R. Membrane Metallo-Endopeptidase (Neprilysin) Regulates Inflammatory Response and Insulin Signaling in White Preadipocytes. *Mol. Metab.* **2019**, *22*, 21–36. [[CrossRef](#)] [[PubMed](#)]
27. Pope, D.; Madura, J.D.; Cascio, M. β -Amyloid and Neprilysin Computational Studies Identify Critical Residues Implicated in Binding Specificity. *J. Chem. Inf. Model.* **2014**, *54*, 1157–1165. [[CrossRef](#)] [[PubMed](#)]
28. Shanmuganathan, B.; Suryanarayanan, V.; Sathya, S.; Narenkumar, M.; Singh, S.K.; Ruckmani, K.; Pandima Devi, K. Anti-Amyloidogenic and Anti-Apoptotic Effect of α -Bisabolol against $A\beta$ Induced Neurotoxicity in PC12 Cells. *Eur. J. Med. Chem.* **2018**, *143*, 1196–1207. [[CrossRef](#)] [[PubMed](#)]
29. Ling, S.S.M.; Lilyanna, S.; Ng, J.Y.X.; Chong, J.P.C.; Lin, Q.; Yong, X.E.; Lim, T.K.; Lin, Q.; Richards, A.M.; Liew, O.W. Multiple Circulating Forms of Neprilysin Detected with Novel Epitope-Directed Monoclonal Antibodies. *Cell. Mol. Life Sci.* **2024**, *81*, 42. [[CrossRef](#)] [[PubMed](#)]
30. Moss, S.; Subramanian, V.; Acharya, K.R. High-Resolution Crystal Structure of Substrate-Free Human Neprilysin. *J. Struct. Biol.* **2018**, *204*, 19–25. [[CrossRef](#)]
31. Bayes-Genis, A.; Barallat, J.; Richards, A.M. A Test in Context: Neprilysin. *J. Am. Coll. Cardiol.* **2016**, *68*, 639–653. [[CrossRef](#)] [[PubMed](#)]
32. Oefner, C.; D'Arcy, A.; Hennig, M.; Winkler, F.K.; Dale, G.E. Structure of Human Neutral Endopeptidase (Neprilysin) Complexed with Phosphoramidon. *J. Mol. Biol.* **2000**, *296*, 341–349. [[CrossRef](#)] [[PubMed](#)]
33. Zhang, H.; Li, X.-J.; Martin, D.B.; Aebersold, R. Identification and Quantification of N-Linked Glycoproteins Using Hydrazide Chemistry, Stable Isotope Labeling and Mass Spectrometry. *Nat. Biotechnol.* **2003**, *21*, 660–666. [[CrossRef](#)] [[PubMed](#)]
34. Sato, B.; Katagiri, Y.U.; Iijima, K.; Yamada, H.; Ito, S.; Kawasaki, N.; Okita, H.; Fujimoto, J.; Kiyokawa, N. The Human CD10 Lacking an N-Glycan at Asn628 Is Deficient in Surface Expression and Neutral Endopeptidase Activity. *Biochim. Biophys. Acta (BBA) Gen. Subj.* **2012**, *1820*, 1715–1723. [[CrossRef](#)] [[PubMed](#)]
35. Deeb, S.J.; Cox, J.; Schmidt-Supprian, M.; Mann, M. N-Linked Glycosylation Enrichment for in-Depth Cell Surface Proteomics of Diffuse Large b-Cell Lymphoma Subtypes. *Mol. Cell. Proteom.* **2014**, *13*, 240–251. [[CrossRef](#)] [[PubMed](#)]
36. Miners, J.S.; Van Helmond, Z.; Kehoe, P.G.; Love, S. Changes with Age in the Activities of β -Secretase and the $A\beta$ -Degrading Enzymes Neprilysin, Insulin-Degrading Enzyme and Angiotensin-Converting Enzyme. *Brain Pathol.* **2010**, *20*, 794–802. [[CrossRef](#)] [[PubMed](#)]
37. Shirotani, K.; Tsubuki, S.; Iwata, N.; Takaki, Y.; Harigaya, W.; Maruyama, K.; Kiryu-Seo, S.; Kiyama, H.; Iwata, H.; Tomita, T.; et al. Neprilysin Degrades Both Amyloid β Peptides 1–40 and 1–42 Most Rapidly and Efficiently among Thiorphan- and Phosphoramidon-Sensitive Endopeptidases. *J. Biol. Chem.* **2001**, *276*, 21895–21901. [[CrossRef](#)] [[PubMed](#)]
38. Iwata, N.; Mizukami, H.; Shirotani, K.; Takaki, Y.; Muramatsu, S.; Lu, B.; Gerard, N.P.; Gerard, C.; Ozawa, K.; Saido, T.C. Presynaptic Localization of Neprilysin Contributes to Efficient Clearance of Amyloid- β Peptide in Mouse Brain. *J. Neurosci.* **2004**, *24*, 991–998. [[CrossRef](#)]
39. Iwata, N.; Tsubuki, S.; Hama, E.; Takaki, Y.; Shirotani, K.; Saido, T.C. Reply to: “Clearance of Amyloid β -Peptide from Brain: Transport or Metabolism?”. *Nat. Med.* **2000**, *6*, 718–719. [[CrossRef](#)]
40. Iwata, N.; Tsubuki, S.; Takaki, Y.; Shirotani, K.; Lu, B.; Gerard, N.P.; Gerard, C.; Hama, E.; Lee, H.-J.; Saido, T.C. Metabolic Regulation of Brain $A\beta$ by Neprilysin. *Science* **2001**, *292*, 1550–1552. [[CrossRef](#)]
41. El-Amouri, S.S.; Zhu, H.; Yu, J.; Marr, R.; Verma, I.M.; Kindy, M.S. Neprilysin: An Enzyme Candidate to Slow the Progression of Alzheimer's Disease. *Am. J. Pathol.* **2008**, *172*, 1342–1354. [[CrossRef](#)]
42. Tampellini, D.; Rahman, N.; Lin, M.T.; Capetillo-Zarate, E.; Gouras, G.K. Impaired β -Amyloid Secretion in Alzheimer's Disease Pathogenesis. *J. Neurosci.* **2011**, *31*, 15384–15390. [[CrossRef](#)] [[PubMed](#)]
43. Li, Y.; Wang, J.; Liu, J.; Liu, F. A Novel System for in Vivo Neprilysin Gene Delivery Using a Syringe Electrode. *J. Neurosci. Methods* **2010**, *193*, 226–231. [[CrossRef](#)] [[PubMed](#)]
44. Marr, R.A.; Guan, H.; Rockenstein, E.; Kindy, M.; Gage, F.H.; Verma, I.; Masliah, E.; Hersh, L.B. Neprilysin Regulates Amyloid β Peptide Levels. *J. Mol. Neurosci.* **2004**, *22*, 5–11. [[CrossRef](#)] [[PubMed](#)]
45. Hemming, M.L.; Patterson, M.; Reske-Nielsen, C.; Lin, L.; Isacson, O.; Selkoe, D.J. Reducing Amyloid Plaque Burden via Ex Vivo Gene Delivery of an $A\beta$ -Degrading Protease: A Novel Therapeutic Approach to Alzheimer Disease. *PLoS Med.* **2007**, *4*, e262. [[CrossRef](#)] [[PubMed](#)]
46. Guan, H.; Liu, Y.; Daily, A.; Police, S.; Kim, M.-H.; Oddo, S.; LaFerla, F.M.; Pauly, J.R.; Murphy, M.P.; Hersh, L.B. Peripherally Expressed Neprilysin Reduces Brain Amyloid Burden: A Novel Approach for Treating Alzheimer's Disease. *J. Neurosci. Res.* **2009**, *87*, 1462–1473. [[CrossRef](#)] [[PubMed](#)]
47. Liu, Y.; Studzinski, C.; Beckett, T.; Guan, H.; Hersh, M.A.; Murphy, M.P.; Klein, R.; Hersh, L.B. Expression of Neprilysin in Skeletal Muscle Reduces Amyloid Burden in a Transgenic Mouse Model of Alzheimer Disease. *Mol. Ther.* **2009**, *17*, 1381–1386. [[CrossRef](#)] [[PubMed](#)]
48. Liu, Y.; Studzinski, C.; Beckett, T.; Murphy, M.P.; Klein, R.L.; Hersh, L.B. Circulating Neprilysin Clears Brain Amyloid. *Mol. Cell. Neurosci.* **2010**, *45*, 101–107. [[CrossRef](#)] [[PubMed](#)]
49. Spencer, B.; Marr, R.A.; Gindi, R.; Potkar, R.; Michael, S.; Adame, A.; Rockenstein, E.; Verma, I.M.; Masliah, E. Peripheral Delivery of a CNS Targeted, Metallo-Protease Reduces $A\beta$ Toxicity in a Mouse Model of Alzheimer's Disease. *PLoS ONE* **2011**, *6*, e16575. [[CrossRef](#)]

50. Roques, B.P.; Noble, F.; Daugé, V.; Fournié-Zaluski, M.C.; Beaumont, A. Neutral Endopeptidase 24.11: Structure, Inhibition, and Experimental and Clinical Pharmacology. *Pharmacol. Rev.* **1993**, *45*, 87–146.
51. Iijima-Ando, K.; Hearn, S.A.; Granger, L.; Shenton, C.; Gatt, A.; Chiang, H.-C.; Hakker, I.; Zhong, Y.; Iijima, K. Overexpression of Nephilysin Reduces Alzheimer Amyloid-B42 (A β 42)-Induced Neuron Loss and Intraneuronal A β 42 Deposits but Causes a Reduction in Camp-Responsive Element-Binding Protein-Mediated Transcription, Age-Dependent Axon Pathology, and Premature Death in *Drosophila*. *J. Biol. Chem.* **2008**, *283*, 19066–19076. [[CrossRef](#)] [[PubMed](#)]
52. Nagore, P.; Lokhande, P.; Mujawar, H. In-Vitro Bioevaluation, Pharmacokinetics and Molecular Docking Study of Unexplored Bisabolol-Rich *Curcuma Inodora* Blatt. Essential Oil from Konkan Region: A Biodiversity Hotspot. *Plant Sci. Today* **2023**, *10*, 223–231. [[CrossRef](#)]
53. Nazarinia, D.; Moslehi, A.; Hashemi, P. (-)- α -Bisabolol Exerts Neuroprotective Effects against Pentylentetrazole-Induced Seizures in Rats by Targeting Inflammation and Oxidative Stress. *Physiol. Behav.* **2023**, *272*, 114351. [[CrossRef](#)] [[PubMed](#)]
54. Kim, S.; Yu, S.; Kim, J.; Khaliq, N.U.; Choi, W.I.; Kim, H.; Sung, D. Facile Fabrication of α -Bisabolol Nanoparticles with Improved Antioxidant and Antibacterial Effects. *Antioxidants* **2023**, *12*, 207. [[CrossRef](#)] [[PubMed](#)]
55. Kamatou, G.P.P.; Viljoen, A.M. A Review of the Application and Pharmacological Properties of α -Bisabolol and α -Bisabolol-Rich Oils. *J. Am. Oil Chem. Soc.* **2010**, *87*, 1–7. [[CrossRef](#)]
56. Eddin, L.B.; Jha, N.K.; Goyal, S.N.; Agrawal, Y.O.; Subramanya, S.B.; Bastaki, S.M.A.; Ojha, S. Health Benefits, Pharmacological Effects, Molecular Mechanisms, and Therapeutic Potential of α -Bisabolol. *Nutrients* **2022**, *14*, 1370. [[CrossRef](#)] [[PubMed](#)]
57. Fernandes, M.Y.D.; Carmo, M.R.S.d.; Fonteles, A.A.; Neves, J.C.d.S.; Silva, A.T.A.d.; Pereira, J.F.; Ferreira, E.d.O.; Lima, N.M.R.d.; Neves, K.R.T.; Andrade, G.M.d. (-)- α -Bisabolol Prevents Neuronal Damage and Memory Deficits through Reduction of Proinflammatory Markers Induced by Permanent Focal Cerebral Ischemia in Mice. *Eur. J. Pharmacol.* **2019**, *842*, 270–280. [[CrossRef](#)] [[PubMed](#)]
58. Braga, P.C.; Dal Sasso, M.; Fonti, E.; Culici, M. Antioxidant Activity of Bisabolol: Inhibitory Effects on Chemiluminescence of Human Neutrophil Bursts and Cell-Free Systems. *Pharmacology* **2009**, *83*, 110–115. [[CrossRef](#)] [[PubMed](#)]
59. Zargarani, A.; Borhani Haghighi, A.; Faridi, P.; Daneshamouz, S.; Kordafshari, G.; Mohagheghzadeh, A. Potential Effect and Mechanism of Action of Topical Chamomile (*Matricaria chamomilla* L.) Oil on Migraine Headache: A Medical Hypothesis. *Med. Hypotheses* **2014**, *83*, 566–569. [[CrossRef](#)]
60. Nascimento, T.V.C. Evidence for the Involvement of TNF- α and IL-1 β in the Antinociceptive and Anti-Inflammatory Activity of *Stachys lavandulifolia* Vahl. (Lamiaceae) Essential Oil and (-)- α -Bisabolol, Its Main Compound, in Mice. *J. Ethnopharmacol.* **2016**, *191*, 9–18.
61. Sathya, S.; Shanmuganathan, B.; Devi, K.P. Deciphering the Anti-Apoptotic Potential of α -Bisabolol Loaded Solid Lipid Nanoparticles against A β Induced Neurotoxicity in Neuro-2a Cells. *Colloids Surf. B Biointerfaces* **2020**, *190*, 110948. [[CrossRef](#)] [[PubMed](#)]
62. Jeyakumar, M.; Sathya, S.; Gandhi, S.; Tharra, P.; Suryanarayanan, V.; Singh, S.K.; Baire, B.; Pandima Devi, K. α -Bisabolol β -D-Fucopyranoside as a Potential Modulator of β -Amyloid Peptide Induced Neurotoxicity: An in vitro & in silico study. *Bioorganic Chem.* **2019**, *88*, 102935. [[CrossRef](#)] [[PubMed](#)]
63. UniProt Consortium. UniProt: The Universal Protein Knowledgebase in 2023. *Nucleic Acids Res.* **2023**, *51*, D523–D531. [[CrossRef](#)] [[PubMed](#)]
64. Sigrist, C.J.A.; de Castro, E.; Cerutti, L.; Cucho, B.A.; Hulo, N.; Bridge, A.; Bougueleret, L.; Xenarios, I. New and Continuing Developments at PROSITE. *Nucleic Acids Res.* **2013**, *41*, D344–D347. [[CrossRef](#)] [[PubMed](#)]
65. Lu, S.; Wang, J.; Chitsaz, F.; Derbyshire, M.K.; Geer, R.C.; Gonzales, N.R.; Gwadz, M.; Hurwitz, D.I.; Marchler, G.H.; Song, J.S.; et al. CDD/SPARCLE: The Conserved Domain Database in 2020. *Nucleic Acids Res.* **2020**, *48*, D265–D268. [[CrossRef](#)] [[PubMed](#)]
66. Blum, M.; Chang, H.-Y.; Chuguransky, S.; Grego, T.; Kandasamy, S.; Mitchell, A.; Nuka, G.; Paysan-Lafosse, T.; Qureshi, M.; Raj, S.; et al. The InterPro Protein Families and Domains Database: 20 Years On. *Nucleic Acids Res.* **2021**, *49*, D344–D354. [[CrossRef](#)] [[PubMed](#)]
67. Webb, B.; Sali, A. Comparative Protein Structure Modeling Using MODELLER. *Curr. Protoc. Bioinform.* **2016**, *54*, 5.6.1–5.6.37. [[CrossRef](#)] [[PubMed](#)]
68. Camacho, C.; Boratyn, G.M.; Joukov, V.; Vera Alvarez, R.; Madden, T.L. ElasticBLAST: Accelerating Sequence Search via Cloud Computing. *BMC Bioinform.* **2023**, *24*, 117. [[CrossRef](#)] [[PubMed](#)]
69. Altschul, S.F.; Madden, T.L.; Schäffer, A.A.; Zhang, J.; Zhang, Z.; Miller, W.; Lipman, D.J. Gapped BLAST and PSI-BLAST: A New Generation of Protein Database Search Programs. *Nucleic Acids Res.* **1997**, *25*, 3389–3402. [[CrossRef](#)]
70. Burley, S.K.; Bhikadiya, C.; Bi, C.; Bittrich, S.; Chen, L.; Crichlow, G.V.; Christie, C.H.; Dalenberg, K.; Di Costanzo, L.; Duarte, J.M.; et al. RCSB Protein Data Bank: Powerful New Tools for Exploring 3D Structures of Biological Macromolecules for Basic and Applied Research and Education in Fundamental Biology, Biomedicine, Biotechnology, Bioengineering and Energy Sciences. *Nucleic Acids Res.* **2021**, *49*, D437–D451. [[CrossRef](#)]
71. Moss, S.; Subramanian, V.; Acharya, K.R. Crystal Structure of Peptide-Bound Nephilysin Reveals Key Binding Interactions. *FEBS Lett.* **2020**, *594*, 327–336. [[CrossRef](#)]
72. Shen, M.; Sali, A. Statistical Potential for Assessment and Prediction of Protein Structures. *Protein Sci.* **2006**, *15*, 2507–2524. [[CrossRef](#)]

73. Chen, V.B.; Arendall, W.B.; Headd, J.J.; Keedy, D.A.; Immormino, R.M.; Kapral, G.J.; Murray, L.W.; Richardson, J.S.; Richardson, D.C. MolProbity: All-Atom Structure Validation for Macromolecular Crystallography. *Acta Crystallogr. D Biol. Crystallogr.* **2010**, *66*, 12–21. [[CrossRef](#)] [[PubMed](#)]
74. Davis, I.W.; Leaver-Fay, A.; Chen, V.B.; Block, J.N.; Kapral, G.J.; Wang, X.; Murray, L.W.; Arendall, W.B.; Snoeyink, J.; Richardson, J.S.; et al. MolProbity: All-Atom Contacts and Structure Validation for Proteins and Nucleic Acids. *Nucleic Acids Res.* **2007**, *35*, W375–W383. [[CrossRef](#)]
75. Prisant, M.G.; Williams, C.J.; Chen, V.B.; Richardson, J.S.; Richardson, D.C. New Tools in MolProbity Validation: CaBLAM for CryoEM Backbone, UnDowser to Rethink “Waters,” and NGL Viewer to Recapture Online 3D Graphics. *Protein Sci.* **2020**, *29*, 315–329. [[CrossRef](#)]
76. Williams, C.J.; Headd, J.J.; Moriarty, N.W.; Prisant, M.G.; Videau, L.L.; Deis, L.N.; Verma, V.; Keedy, D.A.; Hintze, B.J.; Chen, V.B.; et al. MolProbity: More and Better Reference Data for Improved All-Atom Structure Validation. *Protein Sci.* **2018**, *27*, 293–315. [[CrossRef](#)]
77. Volkamer, A.; Kuhn, D.; Rippmann, F.; Rarey, M. DoGSiteScorer: A Web Server for Automatic Binding Site Prediction, Analysis and Druggability Assessment. *Bioinformatics* **2012**, *28*, 2074–2075. [[CrossRef](#)] [[PubMed](#)]
78. Tian, W.; Chen, C.; Lei, X.; Zhao, J.; Liang, J. CASTp 3.0: Computed Atlas of Surface Topography of Proteins. *Nucleic Acids Res.* **2018**, *46*, W363–W367. [[CrossRef](#)] [[PubMed](#)]
79. da Cruz Freire, J.E.; Júnior, J.E.M.; Pinheiro, D.P.; da Cruz Paiva Lima, G.E.; do Amaral, C.L.; Veras, V.R.; Madeira, M.P.; Freire, E.B.L.; Ozório, R.G.; Fernandes, V.O.; et al. Evaluation of the Anti-Diabetic Drug Sitagliptin as a Novel Attenuate to SARS-CoV-2 Evidence-Based *in Silico*: Molecular Docking and Molecular Dynamics. *3 Biotech* **2022**, *12*, 344. [[CrossRef](#)]
80. Gonzatti, M.B.; Júnior, J.E.M.; Rocha, A.J.; de Oliveira, J.S.; Evangelista, A.J.d.J.; Fonseca, F.M.P.; Ceccatto, V.M.; de Oliveira, A.C.; da Cruz Freire, J.E. Mechanism of Molecular Interaction of Sitagliptin with Human DPP4 Enzyme—New Insights. *Adv. Med. Sci.* **2023**, *68*, 402–408. [[CrossRef](#)]
81. Eberhardt, J.; Santos-Martins, D.; Tillack, A.F.; Forli, S. AutoDock Vina 1.2.0: New Docking Methods, Expanded Force Field, and Python Bindings. *J. Chem. Inf. Model.* **2021**, *61*, 3891–3898. [[CrossRef](#)]
82. Humphrey, W.; Dalke, A.; Schulten, K. VMD: Visual Molecular Dynamics. *J. Mol. Graph.* **1996**, *14*, 33–38. [[CrossRef](#)] [[PubMed](#)]
83. Abraham, M.J.; Murtola, T.; Schulz, R.; Páll, S.; Smith, J.C.; Hess, B.; Lindahl, E. GROMACS: High Performance Molecular Simulations through Multi-Level Parallelism from Laptops to Supercomputers. *SoftwareX* **2015**, *1*, 19–25. [[CrossRef](#)]
84. Essmann, U.; Perera, L.; Berkowitz, M.L.; Darden, T.; Lee, H.; Pedersen, L.G. A Smooth Particle Mesh Ewald Method. *J. Chem. Phys.* **1995**, *103*, 8577–8593. [[CrossRef](#)]
85. Berendsen, H.J.C.; Postma, J.P.M.; van Gunsteren, W.F.; DiNola, A.; Haak, J.R. Molecular Dynamics with Coupling to an External Bath. *J. Chem. Phys.* **1984**, *81*, 3684–3690. [[CrossRef](#)]
86. Hess, B. P-LINCS: A Parallel Linear Constraint Solver for Molecular Simulation. *J. Chem. Theory Comput.* **2008**, *4*, 116–122. [[CrossRef](#)] [[PubMed](#)]
87. Schiering, N.; D’Arcy, A.; Villard, F.; Ramage, P.; Logel, C.; Cumin, F.; Ksander, G.M.; Wiesmann, C.; Karki, R.G.; Mogi, M. Structure of Nephilysin in Complex with the Active Metabolite of Sacubitril. *Sci. Rep.* **2016**, *6*, 27909. [[CrossRef](#)]
88. Pankow, K.; Schwiebs, A.; Becker, M.; Siems, W.-E.; Krause, G.; Walther, T. Structural Substrate Conditions Required for Neutral Endopeptidase-Mediated Natriuretic Peptide Degradation. *J. Mol. Biol.* **2009**, *393*, 496–503. [[CrossRef](#)]
89. Salazar, J.; Rojas-Quintero, J.; Cano, C.; Pérez, J.L.; Ramírez, P.; Carrasquero, R.; Torres, W.; Espinoza, C.; Chacín-González, M.; Bermúdez, V. Nephilysin: A Potential Therapeutic Target of Arterial Hypertension? *Curr. Cardiol. Rev.* **2020**, *16*, 25–35. [[CrossRef](#)]
90. Campbell, D.J.; Anastasopoulos, F.; Duncan, A.M.; James, G.M.; Kladis, A.; Briscoe, T.A. Effects of Neutral Endopeptidase Inhibition and Combined Angiotensin Converting Enzyme and Neutral Endopeptidase Inhibition on Angiotensin and Bradykinin Peptides in Rats. *J. Pharmacol. Exp. Ther.* **1998**, *287*, 567–577.
91. Stephenson, S.L.; Kenny, A.J. The Hydrolysis of Alpha-Human Atrial Natriuretic Peptide by Pig Kidney Microvillar Membranes Is Initiated by Endopeptidase-24.11. *Biochem J.* **1987**, *243*, 183–187. [[CrossRef](#)]
92. Jiang, W.; Jiang, H.-F.; Pan, C.-S.; Cai, D.-Y.; Qi, Y.-F.; Pang, Y.-Z.; Tang, C.-S. Relationship between the Contents of Adrenomedullin and Distributions of Neutral Endopeptidase in Blood and Tissues of Spontaneously Hypertensive Rats. *Hypertens. Res.* **2004**, *27*, 109–117. [[CrossRef](#)]
93. Kokkonen, J.O.; Kuoppala, A.; Saarinen, J.; Lindstedt, K.A.; Kovanen, P.T. Kallidin- and Bradykinin-Degrading Pathways in Human Heart: Degradation of Kallidin by Aminopeptidase M-like Activity and Bradykinin by Neutral Endopeptidase. *Circulation* **1999**, *99*, 1984–1990. [[CrossRef](#)] [[PubMed](#)]
94. Mangiafico, S.; Costello-Boerrigter, L.C.; Andersen, I.A.; Cataliotti, A.; Burnett, J.C. Neutral Endopeptidase Inhibition and the Natriuretic Peptide System: An Evolving Strategy in Cardiovascular Therapeutics. *Eur. Heart J.* **2013**, *34*, 886–893c. [[CrossRef](#)] [[PubMed](#)]
95. Abassi, Z.; Golomb, E.; Keiser, H.R. Neutral Endopeptidase Inhibition Increases the Urinary Excretion and Plasma Levels of Endothelin. *Metabolism* **1992**, *41*, 683–685. [[CrossRef](#)]
96. Jaffe, A.S.; Apple, F.S.; Mebazaa, A.; Vodovar, N. Unraveling N-Terminal pro-B-Type Natriuretic Peptide: Another Piece to a Very Complex Puzzle in Heart Failure Patients. *Clin. Chem.* **2015**, *61*, 1016–1018. [[CrossRef](#)] [[PubMed](#)]
97. Riddell, E.; Vader, J.M. Potential Expanded Indications for Nephilysin Inhibitors. *Curr. Heart Fail. Rep.* **2017**, *14*, 134–145. [[CrossRef](#)] [[PubMed](#)]

98. Laws III, J.S.; Shrestha, S.; Smid, S.D. Cannabis Terpenes Display Variable Protective and Anti-Aggregatory Actions against Neurotoxic β Amyloid *in Vitro*: Highlighting the Protective Bioactivity of α -Bisabolol in Motorneuronal-like NSC-34 Cells. *Neuro Toxicol.* **2022**, *90*, 81–87. [[CrossRef](#)] [[PubMed](#)]
99. Sathya, S.; Shanmuganathan, B.; Manirathinam, G.; Ruckmani, K.; Devi, K.P. α -Bisabolol Loaded Solid Lipid Nanoparticles Attenuates A β Aggregation and Protects Neuro-2a Cells from A β Induced Neurotoxicity. *J. Mol. Liq.* **2018**, *264*, 431–441. [[CrossRef](#)]
100. Khan, M.F.; Kundu, D.; Hazra, C.; Patra, S. A Strategic Approach of Enzyme Engineering by Attribute Ranking and Enzyme Immobilization on Zinc Oxide Nanoparticles to Attain Thermostability in Mesophilic *Bacillus Subtilis* Lipase for Detergent Formulation. *Int. J. Biol. Macromol.* **2019**, *136*, 66–82. [[CrossRef](#)]
101. Sharma, U.; Cozier, G.E.; Sturrock, E.D.; Acharya, K.R. Molecular Basis for Omapatrilat and Sampatrilat Binding to Neprilysin—Implications for Dual Inhibitor Design with Angiotensin-Converting Enzyme. *J. Med. Chem.* **2020**, *63*, 5488–5500. [[CrossRef](#)]
102. Verma, R.; Mitchell-Koch, K. In Silico Studies of Small Molecule Interactions with Enzymes Reveal Aspects of Catalytic Function. *Catalysts* **2017**, *7*, 212. [[CrossRef](#)]
103. Agarwal, P.K.; Doucet, N.; Chennubhotla, C.; Ramanathan, A.; Narayanan, C. Conformational Sub-States and Populations in Enzyme Catalysis. *Methods Enzymol.* **2016**, *578*, 273–297. [[CrossRef](#)]
104. Bruice, T.C. Computational Approaches: Reaction Trajectories, Structures, and Atomic Motions. Enzyme Reactions and Proficiency. *Chem. Rev.* **2006**, *106*, 3119–3139. [[CrossRef](#)]
105. Ramanathan, A.; Savol, A.; Burger, V.; Chennubhotla, C.S.; Agarwal, P.K. Protein Conformational Populations and Functionally Relevant Substates. *Acc Chem. Res.* **2014**, *47*, 149–156. [[CrossRef](#)]
106. Laskowski, R.A.; MacArthur, M.W.; Moss, D.S.; Thornton, J.M. PROCHECK: A Program to Check the Stereochemical Quality of Protein Structures. *J. Appl. Cryst.* **1993**, *26*, 283–291. [[CrossRef](#)]
107. Jeyakumar, M.; Sathya, S.; Gandhi, S.; Tharra, P.; Aarthy, M.; Balan, D.J.; Kiruthiga, C.; Baire, B.; Singh, S.K.; Devi, K.P. α -Bisabolol β -D-Fucopyranoside Inhibits β -Amyloid (A β)_{25–35} Induced Oxidative Stress in Neuro-2a Cells via Antioxidant Approaches. *Process Biochem.* **2022**, *121*, 493–503. [[CrossRef](#)]

Disclaimer/Publisher’s Note: The statements, opinions and data contained in all publications are solely those of the individual author(s) and contributor(s) and not of MDPI and/or the editor(s). MDPI and/or the editor(s) disclaim responsibility for any injury to people or property resulting from any ideas, methods, instructions or products referred to in the content.